Experimental and Numerical analysis of a Solar Rotary Kiln for Continuous Treatment of Particle Material

Stefania Tescari, Gkiokchan Moumin, Brendan Bulfin, Lamark de Oliveira, Stefan Schaefer, Nicolas Overbeck, Christian Willsch, Carsten Spenke, Martin Thelen, Martin Roeb, Christian Sattler

German Aerospace Center (DLR), Linder Hoehe, Cologne 51147, Germany, +49 2203 601 2402, stefania.tescari@dlr.de

Abstract. Several energy intensive industrial processes, such as cement production, require particulate material to be treated at high temperatures. Renewable energy could be used to remove the reliance upon fossil fuels in such processes, and of the available technologies concentrated solar energy is perfectly adapted to provide a high temperature energy source. With this objective, the present study focuses on a solar reactor continuously transferring concentrated solar radiation to a bed of flowing particles. Rotary kilns are the chosen concept due to their technical maturity, easy control and simple design. The feasibility of a solar driven rotary kiln has already been proven at lab-scale, with the successful calcination of materials up to a scale of kg/h. The present work describes a large solar rotary kiln able to heat particles to over 1000 °C at flow rates of up to 20 kg/h. The thermal performance of the reactor was evaluated through an on-sun experimental campaign, performed in the high flux solar simulator at the DLR. During one test, 17 kg/h of particles were heated up to 990 °C, with a thermal efficiency of 45 %. An improvement of the efficiency can be obtained by optimizing the reactor. To do this, a numerical model was developed and its parameters fit to the measured data. Simulations were used to quantify the different heat loss mechanisms, and to explore ways of reducing them. The promising experimental results, together with the improvements suggested by the model, provide the basis for an upcoming chemical campaign, where the calcination of $CaCO_3$ and the effect of endothermic reactions on the temperature distribution will be investigated.

INTRODUCITON

Rotary kilns are a common and established device for diverse applications dealing with the thermal treatment of particulate material, with advantages of easy control of operating parameters, such as residence time or temperature, together with a simple design. Although most existing rotary kilns are heated via electricity or fossil fuels, some studies have proposed to supply the required heat via concentrated solar energy.

In the early 80s, Gilles Flamant [1] proposed the first solar rotary kiln for the decarbonation of CaCO3. The reactor consisted of a horizontal refractive cylinder inclined to a few degrees rotating around its axis. The cylinder was open at one side to enable the entrance of concentrated solar radiation. At the other side, particles were continuously fed at a rate of 1.8 kg/h. Rotation and inclination of the reactor move the particles through the cylinder, where they absorbed the incident radiation, heated up to 1000 °C and were calcined. The experimental thermal efficiency, calculated as the energy stored inside the material at operating temperature divided by the incident energy, was between 10-30 %.

Some years later in DLR a rotary kiln was developed for the solar recycling of aluminum [2, 3]. The reactor was made of an insulated silicon carbide crucible of 0.2 m diameter and 0.4 m length. Concentrated solar power, entering through a small aperture at one end of the crucible, varied between 4.6 to 10 kW. These input powers allowed the melting at 800 °C of about 1kg of Aluminum scrap in time ranges of 30 – 360 min, which decreased with the input power [4]. The same reactor was used to demonstrate the melting of salts, such as Na2SO4 at 950 °C using a power of 3.2 kW [3]. Several years later, the reactor was slightly modified and used to cyclically reduce and oxidize cobalt oxide (Co3O4/CoO), for thermochemical storage [5]. In a typical test, a batch of 100-200 g of Co3O4 particles (of 10μm average diameter) were cycled between 1000 °C and 750 °C to complete respectively reduction and oxidation of the material.

Thermochemical energy storage based on the CuO/Cu2O cycle was also studied in a rotary kiln. A ceramic cavity of 0.058 m inner diameter and 0.074 m length was rotated horizontally around its symmetry axis. A batch of about 10 g of CuO powder was heated to 850 °C to allow its reduction [6, 7].

Solar rotary kilns have also been considered as reactors for thermochemical hydrogen production cycles [8, 9] through the dissociation of Zinc oxide. In this case the concept was different as products of the reaction are gaseous and are driven out of the reactor by flowing gas.

At PSI two rotary kilns to effect the calcination of CaCO3 were designed, constructed and tested. Both reactors processed in continuous mode 1-5 mm size particles, one through direct and the other through indirect solar radiation. The first [10] was a 10-kW reactor, of 0.6 m length and 0.35 m diameter, operated in a horizontal position. A conical rotating reaction chamber inclined at 5° transported the reactants from the back feeding zone, to the front reaction zone, where temperatures of 1050-1150 °C were reached. The particles were fed at a rate of 0.6-3 kg/h. The reactor's efficiency, defined as the enthalpy of the calcination reaction at a specified temperature divided by the solar energy input, reached 20 %.

The indirectly irradiated concept was a 10-kW multitube reactor [11, 12]. It consisted of a tilted cylindrical rotating drum lined with ceramic insulation, comprising several tubular reaction chamber placed around the drum. Concentrated solar radiation entered through an 8-cm diameter aperture and heated the cavity and the tubes surface, which transfer the heat to the particles. The drum was about 400 mm in length and diameter. The absorber tubes were in SiC. The particles, fed at a rate of 2-8 kg/h, were heated up to 950-1150 °C and were calcined in a retention time of 5-8 minutes. Reactor efficiency, calculated as the reaction enthalpy divided by the solar incident power, reached over 30 %.

All the described studies proved the concept by successfully treating materials in the kilogram range. The present study progresses to the commercialization of this solar technology by developing a larger system, able to continuously heat several tens of kilograms of particles per hour to more than 1000 °C. The thermal performance of the reactor is identified through on-sun experiments and analyzed through a numerical model. Future applications of the system are the calcination of CaCO3 particles to produce lime (as the major ingredient of cement raw meal) and thermal reduction of redox granules for thermochemical storage.

THE ROTARY KILN

Set-Up Description

The rotary kiln, shown in Fig. 1, consists of a rotating central drum which is fixed axially between a static front housing and a static particle feeder at the back.

The core of the reactor is the crucible (0.75 m length and 0.24 m diameter) made of Inconel, which has good thermal conductivity, is not fragile and can operate at high temperatures.

The crucible is fixed to the outer drum housing through a holding structure made of two aluminum oxide rings inserted into an Inconel structure. In order to reduce heat losses the gap between the drum housing and the crucible is packed with ceramic fibre high temperature insulation in both blanket and loose wool form. The outer colder volume is insulated using high performance blankets (thermal conductivity k of 0.029 W/m·K), while the hottest region is filled with a loose wool (k = 0.27 W/m·K). The outer drum housing is placed on wheels and rotation is controlled by a motor connected to the rear of the drum via a chain and a toothed wheel. Typical rotational speeds of 2 rpm were used, corresponding to 20 % of the maximum power of the motor. An air cooling system was directed onto the front part of the rotating housing, to prevent the electronic system attached there from overheating.

A conical flange (front flange) is mounted to the non-rotating front housing. At its entrance the front flange holds a 5 mm thick quartz window, which seals the system and allows a more controlled gas composition inside the reactor. The window can be flushed by compressed air passing through eight holes pierced on the lateral wall of the front flange.

During a typical experiment, inert bauxite particles were fed inside the reactor. Their physical characteristics are summarized in Tab.1.

TABLE 1. Sintered bauxite particles properties

Quantity	Value	Reference
mean particle diameter (mm)	0.98	Manufacturer data
bulk density (kg/m³)	2040	Manufacturer data
specific heat (J/kg.K)	$9.553 \cdot 10^{-7} \cdot T^3 - 2.913 \cdot 10^{-3} \cdot T^2 + +3.014 \cdot T + 102.1$	Own calculation according to given composition and values from [13]

Particles are conveyed to the crucible through a screw feeder, located at the back of the reactor. The feeder of 150 L capacity has two volume sensors, providing information about the actual filling. Two motors enable the particles movement: one connected to a stirrer, to improve particle flowability and one connected to the screw, controlling the flow of particles from 2 to 65 kg/h. A constant mass flow rate is kept along one experiment. Around the screw auger, a water cooling system keeps the temperature of the tank and the motors below 50 °C.

The complete reactor stands on an aluminum structure that can be inclined up to 6.5°, but was typically held inclined at just 1.6°. Rotational speed and inclination control the residence time of the particles, which flows from the back to the front, where they are collected in a hopper and fall through a pipe to a storage box. At the front opening of the crucible, a second vertical pipe allows gas to exit through the top of the system.

The energy required for heating the particles is provided by a high flux solar simulator [14] located at the DLR, Cologne, Germany. The simulator consists of 10 xenon short arc lamps each with an elliptical reflector. The short wavelength radiation produced by the lamps is concentrated on a target at a distance of about 3 m. The system is able to produce 10-14 kW on a focal surface of about 6 cm radius, with a peak flux of 3400 kW/m². Incident radiation passes through the window and heats the crucible wall and the particles flowing in it.

Temperatures at the rotating crucible wall are monitored by six type-K thermocouples connected to a wireless system. Their position is shown in Fig. 1. One further thermocouple (TC9) inserted through the front flange is placed at the aperture of the hopper to measure the particles temperatures. This thermocouple gives only an indicative value for the particles temperature, as its position can change during an experiment and its contact with the falling particles may not be optimal. In the non-rotating components, several further thermocouples measure the temperature at the feeder, at the window and at the front housing. Moreover an IR camera, with a suitable filter to measure through glass, is used to define a qualitative temperature distribution at different radial positions.

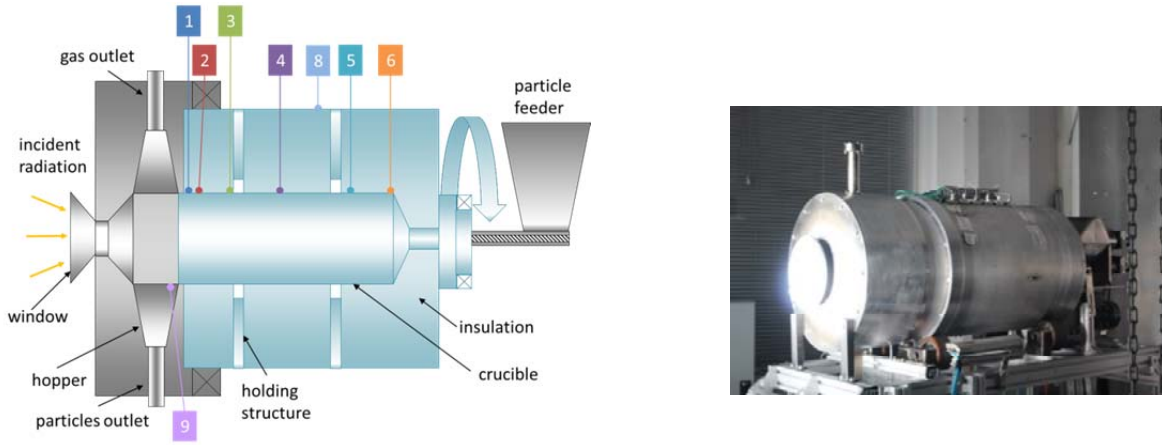

FIGURE 1. a) Scheme of the rotary kiln. Rotating parts are in blue, fixed parts in grey. From the right are shown the screw feeder, the rotating insulated crucible and the fixed front housing, where solar radiation enters and hot particles are extracted. Colored squares show the position of the thermocouples and their identifying numbers. TC1-6 are on the crucible wall, TC8 is on the outer housing and TC9 is at the entrance of the hopper.
b) Picture of the set-up during operation.

Numerical Model

A simple numerical model of the empty reactor is developed to describe the heat flux distribution inside the reactor. The reactor geometry is simplified to be radially symmetric so that it can be simulated in 2D, and was discretized into approximately 10^4 cells, which allowed a mesh-independent solution. A Gaussian shaped incident radiation heats up the inner crucible wall. The heat is distributed inside the reactor through radiation between the walls, the apertures and the particle feeder at the back. Conduction transfers the heat from the walls through the insulation and the crucible holding structure to the housing external wall, where it is dissipated to the environment. The back part of the screw feeder is water-cooled. The model, developed in the commercial software COMSOL(R), calculates the temperature distribution for steady state conditions. Additionally the model was simplified by assuming that at these high temperatures, surface to surface radiation would play a

dominant role in the heat transfer inside the crucible. Therefore, gas flow and convection inside the crucible were omitted from the simulations.

RESULTS

Experimental Results

Some preliminary tests without particles were used to study mechanical stresses and possible problems related to thermal expansion. They showed that the rotation proceeded smoothly also at high temperature and at rotational speeds between 1 and 4 rpm. Particles were then introduced and the temperature distribution on the crucible wall and in the falling particles were monitored through the thermocouples shown in Fig. 1a. Examples of results from the tests are shown in Fig. 2a. During the first 4 tests the reactor could reach maximum temperatures between 940 and 1015 °C, but high heat losses caused a temperature decrease between the hottest point in the reactor and the front exit (ΔT_{Max}) of over 200 °C. The particles temperature, measured at the entrance of the hopper, was close to the front temperature and couldn't exceed 800 °C. An improvement of the insulation in the front of the crucible and on the fix housing, allowed a sharp decrease of the heat losses.

The latter tests (shown in Fig. 2a) show the results for the reactor with improved insulation. ΔT_{Max} decreased by a factor of four, being limited to 48-52 °C. The maximum inner temperature was over 1000°C in most of the tests, with the largest value being 1050 °C. This new insulation allowed a maximum particle temperature of 990 °C. For these tests, incident power and particle flow rates are also shown, in Fig. 2b, which is further explained in the next section.

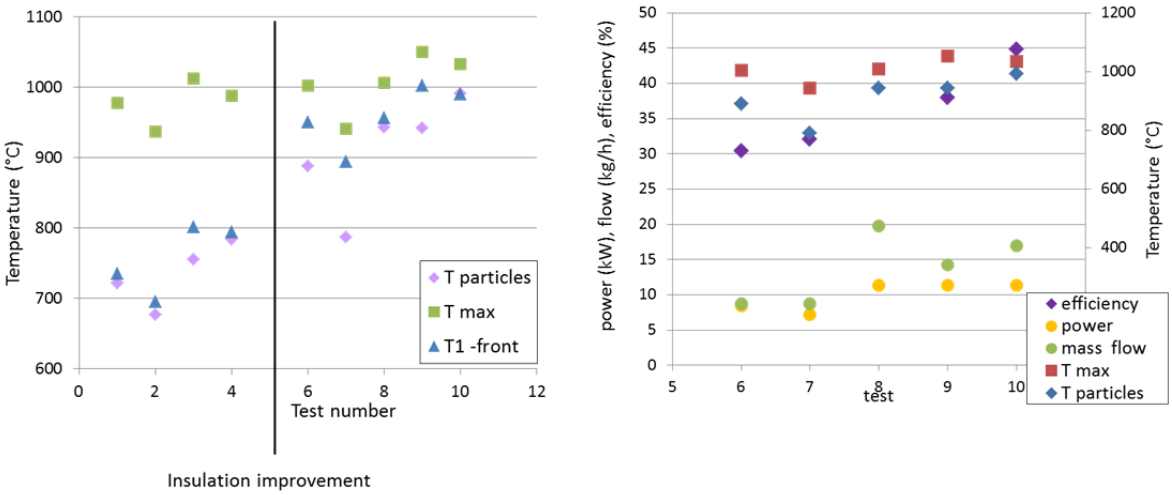

(a) (b)

FIGURE 2. (a) Maximum temperature obtained in ten experiments, in the particles (in purple T9 in Fig. 1), in the crucible wall (in green. Maximum value between T1-T6 in Fig. 1) and in the crucible front (in blue T1 in Fig. 1). (b) performance calculation of the last 5 experiments, after improvement of the insulation

Figure 3 shows the temperature evolution during a test (number nine in Fig. 2). Three phases can be identified, each lasting about two hours: the empty reactor heating to 1000 °C, the steady state with particles flow, and the steady state with the empty reactor. In the first phase, a gradual heat up is achieved by turning on one lamp of the solar simulator every ten minutes. The front of the reactor (TC1-4) heats up faster than the back, due to a higher incident power. TC03 and TC05 are placed close to an alumina ring of the holding structure. The high thermal inertia of the ring causes a delay on heating/cooling of these positions.

In phase two ($t \approx 2$ h), 14.5 kg/h of bauxite particles are fed to the reactor. This causes a sudden decrease of the temperatures recorded at the back of the reactor, while the front temperature remains constant. A constant power of 11.3 kW heats up the particles to a maximum temperature of 1047 °C close to the front of the reactor (TC02). In the foremost part of the crucible the particles are slightly cooled to the exit temperature of 1000 °C. In the last 20 minutes of this phase, the rotational speed of the reactor was increased from 2 to 3 rpm. As a consequence the particles residence time was reduced and the temperature distribution inside the crucible more uniform, i.e. hotter in the back and colder in the front.

In the last phase (t = 4-6 h), the particles flow stops and the reactor emptied. This is evident from a fast heating of the back of the reactor, followed by the front, which reaches almost 1100 °C. To avoid overheating of the reactor, three lamps are turned off and a steady state is reached by the empty reactor. An incident power of 7.1 kW allowed a steady state temperature exceeding 1000 °C in the reactor. Only the very front of the reactor crucible was about 50 °C colder.

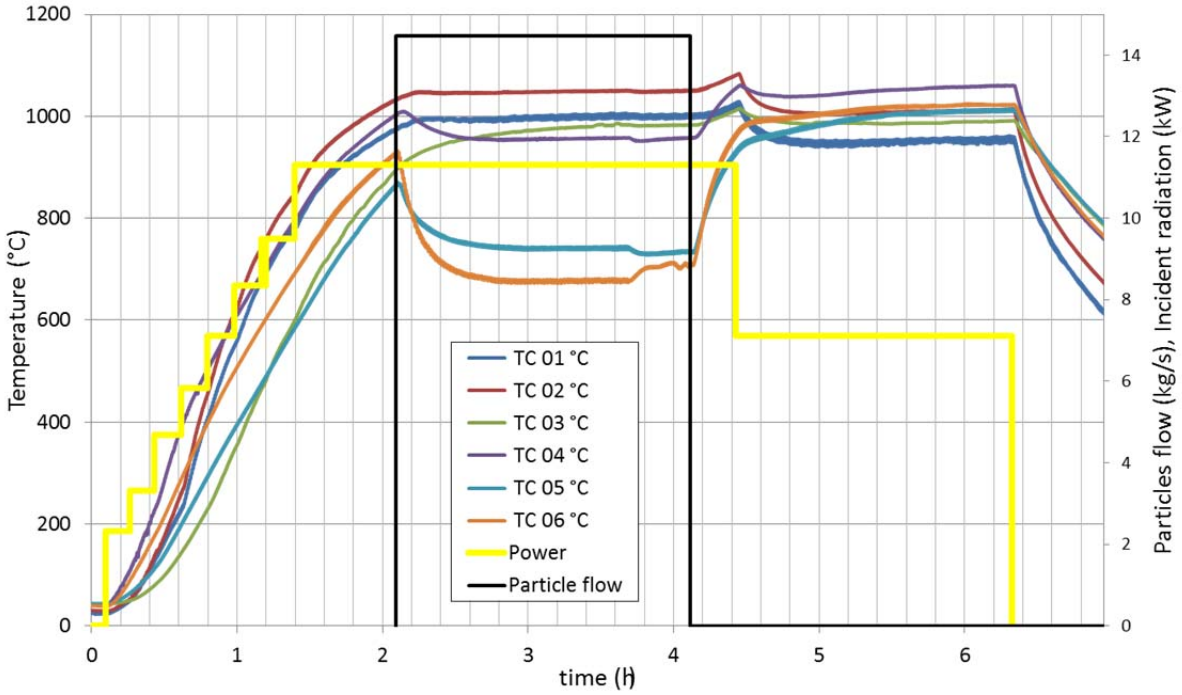

FIGURE 3. Temperature evolution during an experiment. T01 is the closest to the front T06 is on the back. Thermocouple position is described in Fig.1. The right axis describes the power entering the aperture (in yellow) and the particle flow (in black).

The performances of the reactor with the improved insulation are examined in Fig. 2b. The particles rate varies between 9 and 20 kg/h and could be heated up to 1050 °C. Nevertheless, due to higher heat losses in the front of the reactor, the maximum temperature of the particles leaving the crucible was about 1000 °C.

The efficiencies are calculated as $\eta = Q_u/Q_{inc}$, where Q_u is the heat absorbed by the particles to reach the final temperature, and Q_{inc} is the power entering the aperture. As expected, the higher the particles flow, the higher the efficiency and the lower the final temperature. By imposing a minimum outlet temperature of 950 °C, a maximum efficiency of 45 % is reached with a particle flow of 17 kg/h. This flow is limited by the available incident power during the tests. A further increase of the incident power and the particle flow rate would of course lead to further increases in efficiency.

The heat losses were higher than expected, and this limited the efficiency. A numerical model was thus developed to understand better and identify the key factors affecting the heat losses.

Simulation and Comparison

The aim of the simulations is then to analyze the thermal performance and energy balance of the reactor, focusing on the losses through the insulation and housing. For this purpose a reference experimental case is chosen and simulated. The reference case is a steady state condition at a power input of 7.1 kW. The whole experiment can be seen in Fig. 3 of which only the crucible temperatures just before the shutdown of the lamps are considered.

The simulated geometry can be seen in Fig. 4a. The comparison of the experimental and simulated values with the best fitting Gaussian profile can be seen in Fig. 4b. Each point represents one thermocouple. The biggest deviations appear at the front two temperatures. Those are 60 °C and 90 °C lower than in the experiments. The relative error corresponds to 6 % and 9 % for TC 01 and TC 02 respectively. Aside from these values the errors are below 2.5 % and are considered negligible. The explanation for the high deviation in the

front can be that the losses in the front are overestimated by the simulation. The heat flux is imposed on the crucible surface but in reality the flux will also heat the flange and cone in the front part (see Fig. 1a). This will lead to higher temperatures in the front, thus reducing the radiation losses for the front part of the crucible.

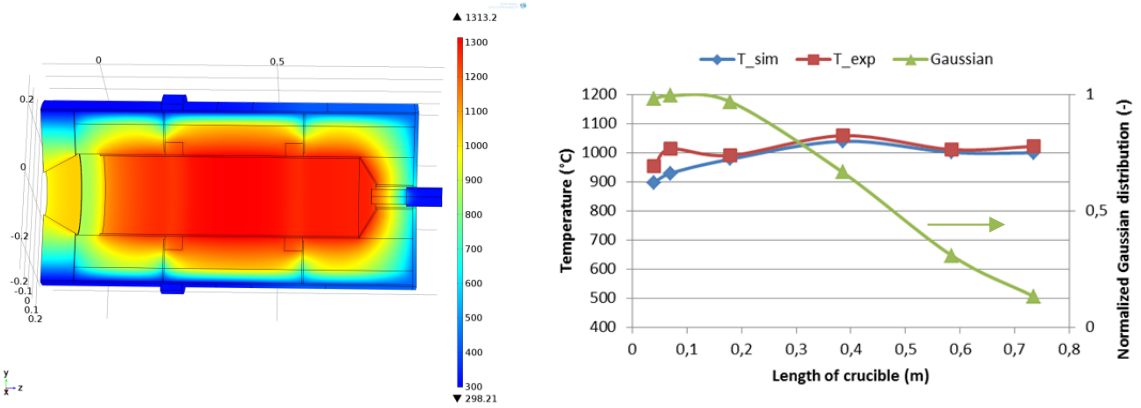

FIGURE 4. a) Geometry and temperature distribution for the steady-state simulation – dimensions in m, temperatures in K b) Comparison of simulated (T_sim) and experimental (T_exp) temperature profile of the crucible

Another reference point between experiments and simulations is the housing temperature. During the experiments, cooling of the housing was achieved using a blower, which was directed at the front part of the reactor (see Fig. 1b). The cooled part reached a temperature of 34 °C whereas the uncooled end of the housing reached 148 °C. The blower creates an impinging jet from a single slot nozzle. This kind of flow is known to yield very high heat transfer coefficients at the flow impact point. However, equations in the literature for the calculation of the coefficient are not valid for the considered set-up since the blower distance divided by slot width is in this case in the range of 1000. Sensitivity analysis showed that the heat transfer coefficient can be varied in a wide range while the change of the temperatures inside is negligible. The coefficient in the simulation was therefore set to 130 W/m²·K in the cooled part and to 3 W/m²·K in the non-cooled part. The emissivity of the housing was set to 0.05 which is a common value for aluminum. With these parameters the simulation yields similar outside temperatures as in the experiment. The deviations are 7 °C and 4 °C for the cooled and uncooled part respectively. With the undertaken simplifications the reactor is still described well enough to gain insights about its thermal performance and possible routes to improvement.

A heat losses analysis shows that conduction heat losses are higher than expected, representing 35 % of the total heat losses. This was proven by the high temperature recorded on the outer reactor wall. The model will next be used to check what kind of measures can be taken to reduce heat losses through the insulation and housing. The main parameters to be varied are the properties of the used insulation and minor constructional changes which can be implemented before the next campaign.

CONCLUSION

In the present study, a large solar rotary kiln able to heat up a flowing bed of particles to a temperature of 1000 °C, was developed and tested. The concentrated solar power was provided by the high flux solar simulator at the DLR, Cologne. Up to 11 kW enters through a quartz window and heats 9-20 kg/h of particles to temperatures over 1000 °C. The hottest point in the crucible was a few cm from the front. A temperature decrease of 50 °C was observed between this point and the front. The thermal efficiency, calculated as the heat absorbed by the particles when heating from ambient to the front temperature divided by the incident power, varied between 30-45 %. A maximum efficiency of 45 % was reached when a particle flow of 17 kg/h was heated up to 990 °C (front temperature). The particles flow rate was set to obtain a front temperature close to 1000 °C. A higher available incident power would allow a higher particle flow rate, and an increased efficiency.

A numerical model was developed to identify and quantify the heat losses. The parameters of the model were changed to best approach the experimental temperature distribution. With the exception of the very front section, the simulated temperatures approached the experimental ones with less than 2.5 % discrepancy. With this model, a heat loss analysis showed that conduction heat losses were higher than expected, representing 35 % of the total and should therefore be limited before the next campaign. The promising experimental results, together with the improvement suggested by the model, provide the basis for an upcoming chemical campaign,

where the effect of endothermic reactions (the calcination of $CaCO_3$ to CaO) on the temperature distribution and energy balance will be investigated.

ACKNOWLEDGMENT

The authors would like to thank the European Commission and the DLR ProgrammdirektionEnergie (PD-E) for partial funding of this work respectively within the Project SOLPART –contract No 654663 under the Horizon 2020 research and innovation programme, and through the Project REDOXSTORE".

We would also like to thank Reiner Buck, Birgit Gobereit and Lars Amsbeck for their share of knowledge and material.

REFERENCES

1. G. Flamant, D. Hernandez, C. Bonet, and J.-P. Traverse, Solar Energy, **24**, 385-395 (1980).
2. K.-H. Funken, M. Roeb, P. Schwarzboezl, and H. Warnecke, Journal of Solar Energy Engineering, **123**, 117-124 (2001).
3. K.-H. Funken, B. Pohlmann, E. Lüpfert, and R. Dominik, Solar Energy, **65**, 25-31 (1999).
4. C. Glasmacher-Remberg, M. Roeb, J. Dersch, R. Schäfer, and K.-H. Funken, AL aluminium and its alloys, **135**, 73 - 77 (2001).
5. M. Neises, S. Tescari, L. de Oliveira, M. Roeb, C. Sattler, and B. Wong, Solar Energy, **86**, 3040-3048 (2012).
6. E. Alonso, C. Pérez-Rábago, J. Licurgo, E. Fuentealba, and C. A. Estrada, Solar Energy, **115**, 297-305 (2015).
7. E. Alonso, C. Pérez-Rábago, J. Licurgo, A. Gallo, E. Fuentealba, and C. A. Estrada, Renewable Energy, **105**, 665-673 (2017).
8. P. Haueter, S. Moeller, R. Palumbo, and A. Steinfeld, Solar Energy, **67**, 161-167 (1999).
9. P. Charvin, S. Abanades, P. Neveu, F. Lemont, and G. Flamant, Chemical Engineering Research and Design, **86**, 1216-1222 (2008).
10. A. Meier, E. Bonaldi, G. M. Cella, W. Lipinski, D. Wuillemin, and R. Palumbo, Energy, **29**, 811–821 (2004).
11. A. Meier, E. Bonaldi, G. M. Cella, W. Lipinski, and D. Wuillemin, Solar Energy, **80**, 1355-1362 (2006).
12. A. Meier, E. Bonaldi, G. M. Cella, and W. Lipinski, Journal of Solar Energy Engineering, **127**, 386–395 (2005).
13. C. E. Wicks and F. E. Block, *Thermodynamic Properties of 65 Elements: Their Oxides, Halides, Carbides and Nitrides*. Vol. 605. 1963: US Government Printing Office.
14. G. Dibowski, A. Neumann, P. Rietbrock, C. Willsch, J.-P. Säck, and K.-H. Funken, 10. Kölner Sonnenkolloquium 2007, Köln